Deletion of a dehydratase important for intracellular growth and cording renders rough *Mycobacterium abscessus* avirulent

Iman Halloum[a], Séverine Carrère-Kremer[b,c], Mickael Blaise[a], Albertus Viljoen[a], Audrey Bernut[a], Vincent Le Moigne[d], Catherine Vilchèze[e,f], Yann Guérardel[g], Georges Lutfalla[h], Jean-Louis Herrmann[d], William R. Jacobs Jr.[e,f,1], and Laurent Kremer[a,i,1]

[a]Centre d'études d'agents Pathogènes et Biotechnologies pour la Santé (CPBS), CNRS Formation de Recherche en Evolution 3689, 34293 Montpellier, France; [b]INSERM U1058, Université de Montpellier, Montpellier 34095, France; [c]Department of Bacteriology–Virology, Centre Hospitalo-Universitaire de Montpellier, Montpellier 34095, France; [d]UMR1173, INSERM, Université de Versailles St. Quentin, 78180 Montigny le Bretonneux, France; [e]Department of Microbiology and Immunology, Albert Einstein College of Medicine, Bronx, NY 10461; [f]Howard Hughes Medical Institute, Albert Einstein College of Medicine, Bronx, NY 10461; [g]University of Lille, CNRS, UMR 8576, Unité de Glycobiologie Structurale et Fonctionnelle (UGSF), 59000 Lille, France; [h]Laboratoire de Dynamique des Interactions Membranaires Normales et Pathologiques, CNRS UMR5235, Université Montpellier, 34293 Montpellier, France; and [i]INSERM, CPBS, 34293 Montpellier, France

Contributed by William R. Jacobs Jr., June 2, 2016 (sent for review February 17, 2016; reviewed by R. Andres Floto and Todd A. Gray)

***Mycobacterium abscessus* (*Mabs*) is a rapidly growing *Mycobacterium* and an emerging pathogen in humans. Transitioning from a smooth (S) high-glycopeptidolipid (GPL) producer to a rough (R) low-GPL producer is associated with increased virulence in zebrafish, which involves the formation of massive serpentine cords, abscesses, and rapid larval death. Generating a cord-deficient *Mabs* mutant would allow us to address the contribution of cording in the physiopathological signs of the R variant. Herein, a deletion mutant of *MAB_4780*, encoding a dehydratase, distinct from the β-hydroxyacyl-ACP dehydratase HadABC complex, was constructed in the R morphotype. This mutant exhibited an alteration of the mycolic acid composition and a pronounced defect in cording. This correlated with an extremely attenuated phenotype not only in wild-type but also in immunocompromised zebrafish embryos lacking either macrophages or neutrophils. The abolition of granuloma formation in embryos infected with the dehydratase mutant was associated with a failure to replicate in macrophages, presumably due to limited inhibition of the phagolysosomal fusion. Overall, these results indicate that MAB_4780 is required for *Mabs* to successfully establish acute and lethal infections. Therefore, targeting MAB_4780 may represent an attractive antivirulence strategy to control *Mabs* infections, refractory to most standard chemotherapeutic interventions. The combination of a dehydratase assay with a high-resolution crystal structure of MAB_4780 opens the way to identify such specific inhibitors.**

M. abscessus | zebrafish | cording | dehydratase | virulence

Microscopic cords, a phenotypic characteristic of *Mycobacterium tuberculosis*, were originally observed by Robert Koch in 1882, but their potential significance in virulence was reported in 1947 by Middlebrook et al. (1). They are made of tight bundles formed by parallel alignments of bacilli and are historically considered as a distinctive trait of *M. tuberculosis*. Their presence in smears from liquid cultures is a reliable criterion for the rapid presumptive identification of *M. tuberculosis* isolates in many laboratories (2, 3). Cord formation correlates with extracellular replication of mycobacteria and can be observed in sputum smears from tuberculosis patients with severe lung cavitation. However, while focusing on the complex network of interactions between intracellular mycobacteria and host cells, most investigators have neglected or underestimated the role of extracellular mycobacteria in pathogenesis (4). Recent studies demonstrated the occurrence of cording in *Mycobacterium marinum* (5) and in several nontuberculous mycobacteria (NTM) distantly related to *M. tuberculosis*, including *Mycobacterium abscessus* (*Mabs*) (6).

Mabs is one of the most pathogenic and drug-resistant rapid-growing mycobacterial species (7, 8) and accounts for 10% of the NTM-induced lung infections in several countries (9). It infects lungs of patients with underlying lung disorders such as cystic fibrosis (10) but also causes skin and soft tissue infections in immunocompetent individuals (11). *Mabs* can exhibit a rough (R) or a smooth (S) morphotype, depending on the absence or presence of surface-associated glycopeptidolipids (GPLs) (12, 13). R strains possess mutations in the *gpl* locus that lead to a defect in GPL production/transport and are also associated with the ability to produce cords in vitro, as recently demonstrated in clinical isolates of *Mabs* (14) as well as in *Mycobacterium* spp. *bolletii* (15), a subspecies of the *Mabs* complex. We recently used the zebrafish embryo as a tractable infection model to study, at a spatiotemporal level, the physiopathology of *Mabs* infection and demonstrated the high propensity of virulent R variant *Mabs* to produce cords in vivo (16, 17). We showed that extracellular cording is an example of morphological plasticity allowing bacteria to escape the host immune system. Therefore, interfering with cording could preclude the establishment of a lethal infection and could be viewed as a

Significance

***Mycobacterium abscessus* is currently the most frequently isolated rapid-growing mycobacterium in human pathology and is responsible for devastating pulmonary infections in cystic fibrosis patients. It commutes from a nonvirulent smooth to a virulent rough morphotype. The latter produces characteristic serpentine cords that often associate with severe infections, but the molecular basis and contribution of cording in the physiopathology of the infection remain obscure. Herein, we characterized a dehydratase and found it to be required for cording. We demonstrate that the absence of this dehydratase correlates with an extremely attenuated phenotype in immunocompetent and immunocompromised zebrafish. Therefore, targeting the dehydratase may open the way to antivirulence strategies to control *M. abscessus*, notorious for being one of the most drug-resistant mycobacterial species.**

Author contributions: I.H., S.C.-K., M.B., A.V., A.B., and L.K. designed research; I.H., S.C.-K., M.B., A.V., A.B., V.L.M., and L.K. performed research; V.L.M., C.V., Y.G., G.L., J.-L.H., and W.R.J. contributed new reagents/analytic tools; I.H., S.C.-K., M.B., A.V., A.B., C.V., Y.G., G.L., J.-L.H., W.R.J., and L.K. analyzed data; and I.H. and L.K. wrote the paper.

Reviewers: R.A.F., Cambridge Institute for Medical Research; and T.A.G., Genomics Institute.

The authors declare no conflict of interest.

Data deposition: The atomic coordinates and structure factors have been deposited in the Protein Data Bank, www.pdb.org (PDB ID code 5I7N).

[1]To whom correspondence may be addressed. Email: laurent.kremer@cpbs.cnrs.fr or jacobsw@hhmi.org.

This article contains supporting information online at www.pnas.org/lookup/suppl/doi:10.1073/pnas.1605477113/-/DCSupplemental.

therapeutic or prophylactic strategy for *Mabs* (8). If identified, the determinants controlling cording may represent drug targets for innovative therapeutic approaches and would undoubtedly add new insights into the pathogenicity of *Mabs*-driven infections. However, whereas the search for genetic determinants of cording has mainly focused on *M. tuberculosis* (18), those involved in cording in NTM remain unknown.

Mutations in *hadC*, encoding a component of the HadBC dehydratase complex of the mycolic acid biosynthesis machinery, have been associated with high resistance levels to the antitubercular drug thiacetazone (TAC) in *M. tuberculosis* (19–21). Moreover, deletion of *hadC* in *M. tuberculosis* correlates with a loss of cording and attenuation of virulence in infected mice (22), thus emphasizing the intimate interplay between TAC resistance, mycolic acid biosynthesis, cording, and virulence. We have previously shown that *Mycobacterium smegmatis* possesses a gene, *MSMEG_6754*, responsible for its remarkable resistance to TAC and involved in mycolic acid metabolism and that disruption of *MSMEG_6754* in *M. smegmatis* was associated with impaired growth in *Acanthamoeba castellanii* (23). Interestingly, *MSMEG_6754* encodes a putative dehydratase and is structurally related to the HadABC complex (23). Blast analyses revealed the presence of genes homologous to *MSMEG_6754* in several NTMs, all of which possess intact *hadABC* genes (23). The presence of such a homolog in *Mabs*, designated *MAB_4780*, prompted us to perform the biochemical/structural characterization of MAB_4780 to investigate its biological function with respect to mycolic acid biosynthesis. We found important roles for this protein in cording and *Mabs* pathogenicity in the zebrafish model.

Results

Enzymatic and Structural Characterization of a Dehydratase from *Mabs*. MAB_4780 shares high identity levels with the *M. tuberculosis* HadA, HadB, and HadC dehydratase subunits. To get functional insights into the enzymatic activity of MAB_4780, the recombinant protein was used in a functional assay. Because the hydratase/dehydratase family members are usually more efficient at catalyzing the hydration reaction when isolated from their complex (24), a hydratase-based assay was set up with *trans*-2-enoyl-CoA substrates exhibiting various chain lengths. Whereas no activity was detected with crotonoyl-CoA (C4), MAB_4780 exhibited a measurable activity in the presence of octanoyl-CoA (C8), which was further increased with dodecenoyl-CoA (C12) (Fig. 1*A*). The specific activities with C8 and C12 were similar to those reported previously with the *M. tuberculosis* HadBC dehydratase of the type II fatty acid synthase (25), suggesting that MAB_4780, like HadBC, is a dehydratase with a substrate preference for long fatty acyl chains.

Because most dehydratases have been found to form homo- or heterodimers (26, 27), we next evaluated the oligomeric state of MAB_4780. The size exclusion chromatography elution profile attests to the presence of a protein of around 70 kDa (Fig. 1*B*). According to the primary sequence, the predicted molecular weight of one monomer is 36.5 kDa, implying that MAB_4780 is very likely to form a dimer in solution. Additionally, we crystallized and solved the structure of MAB_4780 at very high resolution (1.65 Å) (Table S1), in which most residues could be rebuilt, with the exception of the first nine residues of the N terminus and residues 172–180 of the flexible linker. This structure is very similar to the one of the homologous protein in *M. smegmatis* (MSMEG_6754) (23) and to HadAB from *M. smegmatis* (28) (Fig. 1*C*) and *M. tuberculosis* (29). The superposition of the

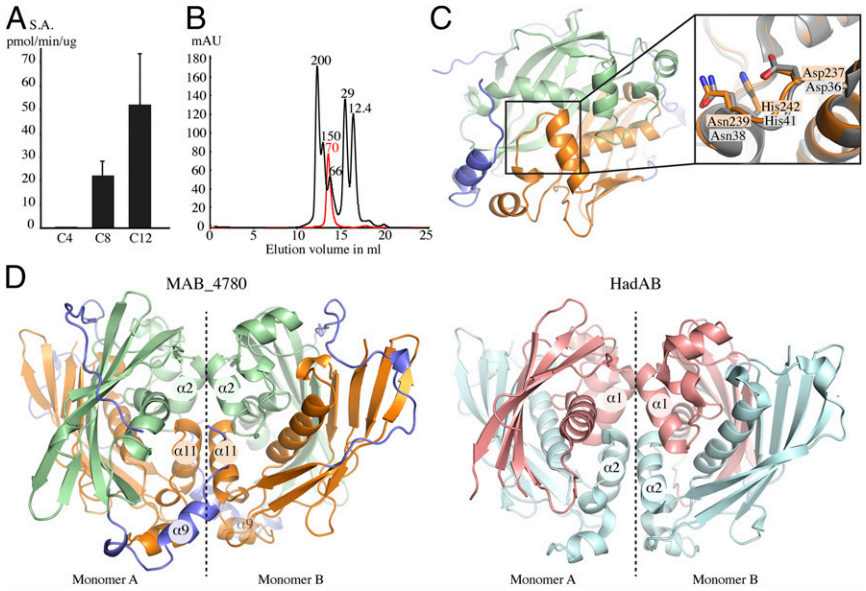

Fig. 1. Enzymatic and structural characterization of MAB_4780. (*A*) The specific activity of MAB_4780 was determined in the presence of *trans*-2-enoyl-CoAs with various fatty acyl chain lengths and expressed in picomole of product formed per minute per microgram of enzyme. C4, C8, and C12 indicate crotonoyl-CoA, *trans*-2-octenoyl-CoA, and *trans*-2-dodecenoyl-CoA, respectively. Error bars represent SDs. (*B*) Oligomeric state of MAB_4780 determined by size exclusion chromatography. The elution profile of the proteins used for the calibration is displayed as a black line, and the elution profile of MAB_4780 is shown in red. Calibration was established using β-amylase (200 kDa), alcohol dehydrogenase (150 kDa), albumin (66 kDa), carbonic anhydrase (29 kDa), and cytochrome C (12.4 kDa), eluting with estimated volumes of 16.1, 15.2, 13.4, 12.6, and 11.9 mL, respectively. The elution volume of MAB_4780 was estimated to 12.7 mL, corresponding to a calculated molecular weight of 70 kDa. (*C*) Schematic representation of the overall monomeric crystal structure of MAB_4780. The N-terminal domain is represented in pale green, the C-terminal domain in orange, and the linker domain surrounding the protein and acting as a belt in blue. The enlarged panel on the side highlights the MAB_4780 catalytic residues (in orange) superposed to the ones of *M. smegmatis* HadAB (in gray; PDB ID code 4rv2). (*D*) Structure of the MAB_4780 homodimer and comparison with the HadAB heterodimer structure. Shown is a representation of one biological unit (homodimer, monomers A and B) of MAB_4780 (with the same color code as in *C*) and one biological unit (heterodimer, monomer A and B) of HadAB (HadB in pale cyan and HadA in salmon). Dashed lines indicate the dimeric interface. The designations of the helices involved in the interface of dimerization are indicated in the circles.

MAB_4780 and HadAB crystal structures indicates that the N-terminal and C-terminal domains of MAB_4780 correspond to the HadA and HadB proteins, respectively. A notable structural difference relies on the existence of a long flexible linker in MAB_4780, absent in HadAB from *M. smegmatis* (Fig. 1*C*). Analysis of the MAB_4780 crystal packing using the proteins, interfaces, structures and assemblies (PISA) server (30) predicts the existence of a stable homodimer. The dimer interface is formed by interactions between helices α2 (R28-A37), α9 (T158-A165) and α11 (R225-A235) of the first monomer and the equivalent helices of the second monomer (Fig. 1*D*). This dimer interface is also conserved in HadAB, where the helix α1 (G21-A31) of HadA and helix α2 (T23-G35) of HadB interact with their corresponding helices of the second monomer. Overall, this indicates that MAB_4780 is a homodimer sharing similar biochemical and structural features with the HadAB/HadBC dehydratases.

Disruption of *MAB_4780* Alters Resistance to TAC and Affects the Mycolic Acid Composition. To decipher the in vivo functions of MAB_4780, the corresponding gene was deleted in the R strain *Mabs* 104536^T. The recombineering method (31) was used to create a mutant with a hygromycin resistance cassette disrupting *MAB_4780* (Fig. 2*A*). A hygromycin-resistant colony was PCR analyzed for correct allelic exchange at the *MAB_4780* locus (Fig. 2*B*). Western blotting using anti-MAB_4780 antibodies highlights the absence of a specific band in the Δ*MAB_4780* strain and the correct complementation using pMV306_*4780* (Fig. 2*C*). As reported earlier for the *M. smegmatis MSMEG_6754* mutant (23), the *MAB_4780* mutant displays increased susceptibility to TAC both on agar plates and broth medium (Table 1). Introduction of pMV306_*4780* partially restored TAC resistance in Δ*MAB_4780* and in Δ*MSMEG_6754* (Table 1), supporting the overlapping functions of MAB_4780 and MSMEG_6754 in TAC resistance.

Susceptibility of Δ*MAB_4780* to detergent was tested on agar plates and in liquid cultures with various SDS concentrations (Fig. S1). Complementation with pMV306_*4780* reversed the susceptibility to the parental levels. This suggests that MAB_4780 plays an important role on the envelope integrity. To confirm the possible involvement of the dehydratase in cell wall-associated lipid biosynthesis, a TLC-based systematic analysis of apolar and polar lipids was performed. Neither the (glyco)lipid nor the GPL patterns of the Δ*MAB_4780* mutant showed major alterations compared with that of the parental and complemented strains (Fig. S2). GC–MS analyses also failed to show important differences in the total fatty acid profiles (Fig. S3). We next determined and compared the mycolic acid composition in both the parental and Δ*MAB_4780* strains. Mass spectrometry and NMR analyses revealed the presence of α- and α′-mycolic acids sharing identical structures in both strains (Figs. S4 and S5). However, labeling the cultures with ^{14}C-acetate, followed by TLC/autoradiography analysis, unraveled a substantial change in the typical α-/α′-mycolic acid ratio (Fig. 2*D*). Whereas α-mycolic acids appeared as the major mycolic acid subclass in the parental R strain, α′ -mycolic acids represented a more prominent mycolic acid subclass in Δ*MAB_4780* and this change was fully restored upon complementation (Fig. 2 *D* and *E*). Because α- and α′-mycolic acids correspond to long-chain ($C_{77–79}$) and short-chain ($C_{62–64}$) mycolic acids, respectively (Fig. 2*F*), an alteration of the α-/α′-mycolic acid ratio in Δ*MAB_4780* may directly impact on the overall cell wall morphology, permeability, and virulence properties of this strain.

MAB_4780 Is Critical for Cording in R *Mabs*. *Mabs* R grows optimally at temperatures ranging from 30 to 37 °C and is characterized by a rough and dry texture on agar plates with prominent cords made of numerous irregular and long serpentine filaments that can be easily observed in liquid medium (Fig. 3) (16). The Δ*MAB_4780* mutant failed to produce these typical cell wall-associated traits, indicating that MAB_4780 plays a central role in *Mabs* cording at 32 °C (Fig. 3). Complementation of the mutant restored cording. All three strains displayed comparable planktonic growth rates in 7H9 broth at different temperatures based on OD_{600} measurements (Fig. S6*A*), on the determination of cfu/mL (Fig. S6*B*), or on the fluorescence intensity of bacilli expressing tdTomato (Fig. S6*C*).

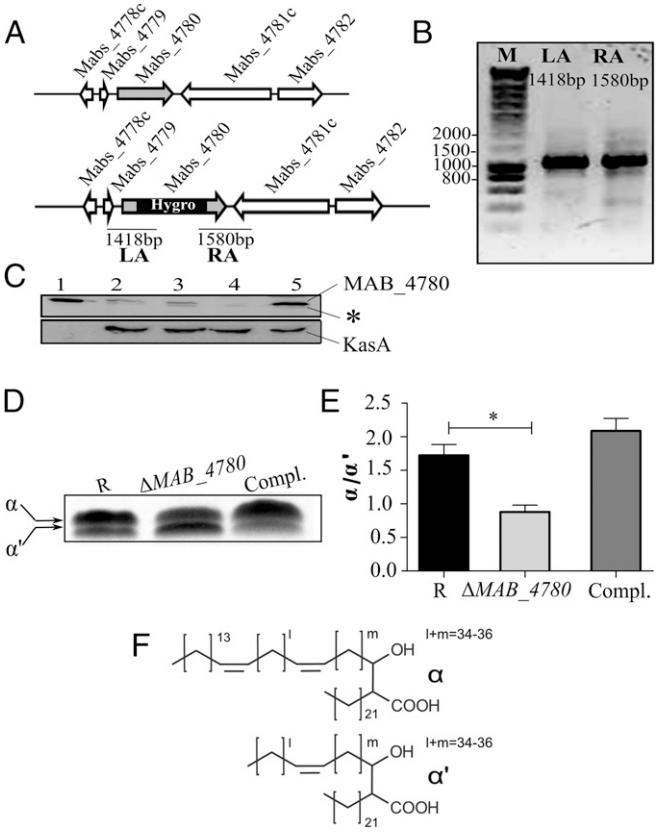

Fig. 2. Interruption of *MAB_4780* in *Mabs* R leads to changes in the mycolic acid profile. (*A*) Genomic organization of the *MAB_4780* locus in *Mabs* CIP104536^T (*Upper*) and schematic representation of the *MAB_4780* locus after disruption with a hygromycin cassette (*Lower*). The primers used for PCR amplifications are indicated by small arrows, and the expected sizes of the left (LA) and right (RA) arms are indicated. (*B*) Agarose gel electrophoresis of the PCR amplified LA and RA products using the genomic DNA from the Δ*MAB_4780* mutant. Identity of the amplicons was verified by DNA sequencing. (*C*) Proper inactivation of *MAB_4780* was further confirmed by Western blotting using mouse anti-MAB_4780 antibodies. The same lysates were also probed with rat anti-KasA antibodies used as loading controls. Lane 1, purified His-tagged MAB_4780 (10 ng); lane 2, crude lysate of *Mabs* S; lane 3, crude lysate of *Mabs* R; lane 4, crude lysate of *Mabs* R Δ*MAB_4780*; lane 5, Δ*MAB_4780* carrying pMV306_*4780* (complemented strain) (35 μg in each lane). An asterisk indicates a cross-reacting band. (*D*) TLC analysis of mycolic acid methyl esters (MAMEs) isolated from logarithmically growing cultures following metabolic labeling with ^{14}C-acetate. After extraction, equal counts (100, 000 cpm) were loaded in each lane, and radiolabeled lipids were separated using petroleum ether/acetone (95:5, vol/vol) before exposure to a film. (*E*) Histograms representing the α/α′-mycolic acid ratio determined from the TLC densitometric analysis. Results are expressed as the means and their SE obtained from three independent experiments. The mean values of the wild-type and mutant strains were compared using a one-tailed Mann–Whitney test. *$P < 0.05$. (*F*) Structure of α and α′-mycolic acids based on MS, NMR, and GC–MS analyses.

Acute Infection Is Highly Compromised in Zebrafish Infected with Δ*MAB_4780*. The virulence of the *Mabs* R strain, compared with that of the S strain, could be due to the loss of GPL or to the massive production of serpentine cords. To distinguish between

Table 1. MICs of TAC in Middlebrook 7H10/OADC agar and cation-adjusted Mueller–Hinton (CaMH) broth

Strain	MIC, μg·mL^{-1}	
	7H10	CaMH
Mabs 104536^{T} (R)	40	150
Δ*MAB_4780*	10–20	37
Δ*MAB_4780* (pMV306_*4780*)	40	83
M. smegmatis mc^{2}155	>50	75
Δ*MSMEG_6754*	<10	0.4
Δ*MSMEG_6754* (pMV306_*4780*)	>50	37

MICs were determined according to the Clinical and Laboratory Standards Institute guidelines (51) used for antimycobacterial susceptibility testing of rapidly growing mycobacteria. The broth microdilution method was used in media with an inoculum of 5×10^5 cfu/mL in the exponential growth phase. We added 100 μL of drug dilutions to 100 μL of bacterial suspension and incubated the mixture at 37 °C for 3 d. MICs were recorded by visual inspection and by absorbance at 560 nm to confirm visual recording.

these two possibilities, we tested the virulence of the cording-defective Δ*MAB_4780* (R background). First, the various strains were inoculated in the yolk sac of zebrafish embryos, previously used as a site of injection of several fast-growing bacteria and resulting in intense bacteraemia and early death of embryos (32, 33). All strains, including the otherwise attenuated *Mabs* S variant, induced a robust infection with unrestricted proliferation, leading to rapid larval death (Fig. 4*A*). Δ*MAB_4780* behaved similarly to its parental and complemented counterparts.

We next investigated whether circulation-injected embryos, which, in contrast to the yolk-injected embryos, possess a myeloid cell-dependent immunity, can resist Δ*MAB_4780* lethal infection. Bacterial suspensions (100–200 cfu) were injected into the caudal vein of embryos at 30 h postfertilization (hpf). As reported earlier, the R variant induced a robust and lethal infection with about 50% mortality of embryos at 9 d post infection (dpi), whereas the S bacteria failed to induce larval mortality (Fig. 4*B*) (16). Δ*MAB_4780* was found to be highly attenuated at levels comparable to the S variant, and complementation fully restored the R virulence phenotype (Fig. 4*B*). Injection of large amounts of Δ*MAB_4780* (up to 2,000 cfu) did not result in increased larval mortality, further emphasizing the extreme attenuated phenotype of Δ*MAB_4780* (Fig. 4*C*). The bacterial loads in *Mabs* S and Δ*MAB_4780*-infected embryos increased only slightly after infection, whereas those in the R variant and complemented infected embryos increased exponentially from 3 dpi to 7 dpi (Fig. 4*D*). Consistent with the very low bacterial burden in the Δ*MAB_4780*-infected embryos, time-lapse imaging revealed the presence of mainly isolated bacteria and very rare infection foci (Fig. 4*E*). In contrast, embryos infected with the parental R and complemented strains harbored massive abscesses and cords, mainly located within the brain (Fig. 4 *E* and *F*) (16). Representative confocal microscopy images revealed highly organized serpentine cord structures of variable sizes, often larger than 100 μm, in fish infected with the R or the complemented strains (Fig. 4*G*). In sharp contrast, only small bacterial aggregates found within macrophages were observed with Δ*MAB_4780* (Fig. 4*G*, *Inset*).

MAB_4780 Is Required for Intracellular Growth and Granuloma Formation. We next determined the proportion of mildly infected (<5 bacteria), moderately infected (5–10 bacteria), and highly infected (>10 bacteria) macrophages in zebrafish. Significantly more macrophages were heavily infected in embryos with the R or the complemented strains, whereas embryos with Δ*MAB_4780* contained more macrophages of the lower infected class (Fig. 5*A*). This intramacrophage growth defect of Δ*MAB_4780* was subsequently confirmed in infected J774 macrophages (Fig. S7*A*). Moreover, the reduced intracellular growth of Δ*MAB_4780* was also found in infected *A. castellanii* (Fig. S7*D*), posited to be a natural environmental host for several NTMs (34). Because inhibition of phagolysosome fusion represents a key strategy used by pathogenic mycobacteria to survive and replicate intracellularly (35), we tested whether the reduced ability of the mutant to grow intracellularly was linked to lysosome-mediated degradation. FITC-labeled bacteria were used to study the localization of the pathogen in acidic compartments in infected J774 macrophages labeled with LysoTracker Red Dye (Fig. S7*B*). Although 47% of the parental bacteria colocalized to acidic vesicles, 64% of Δ*MAB_4780* colocalized with LysoTracker red-positive compartments (Fig. S7*C*) and the complemented strain showed similar colocalization rates to the parental strain.

We next evaluated the impact of defective intracellular replication of Δ*MAB_4780* on its ability to stimulate granuloma formation. Large granuloma-like aggregates containing *Mabs* R could be imaged (Fig. 5*B*), as reported earlier (16). In contrast, Δ*MAB_4780* failed to induce typical structured granulomas (Fig. 5*B*). At 5 dpi, granulomas were present in more than 80% of embryos infected with the R and complemented strains (Fig. 5*C*). In Δ*MAB_4780*-infected embryos, no granulomas were present at 3 dpi but eventually started to appear at 5 dpi in very few numbers and in a very limited proportion of embryos (Fig. 5 *C* and *D*). These results suggest that MAB_4780 plays an important role to avoid lysosome-mediated degradation in macrophages, which compromises survival of Δ*MAB_4780* in macrophages and, as a consequence, granuloma formation.

Cording Is the Hallmark of *M. abscesssus*-Induced Lethal Infection. We next investigated the propensity of Δ*MAB_4780* to produce cords in embryos in the absence of macrophages. Injection of antisense morpholinos against the myeloid transcription factor gene *pu.1* (36) leads to macrophage-depleted embryos without affecting the neutrophils (Fig. S8 *A* and *B*). Following infection and as shown previously (16), 100% of the morphants were heavily infected with the R variant and developed serpentine cords (Fig. 6*A*). Only 23% of the *pu.1* morphants infected with Δ*MAB_4780* exhibited extracellular bacterial structures (Fig. 6*A*), which did not ressemble organized cords and were much smaller in size (Fig. 6*B*). Whereas R infection resulted in 100% of larval killing at 3 dpi, Δ*MAB_4780* infection led to only 20%

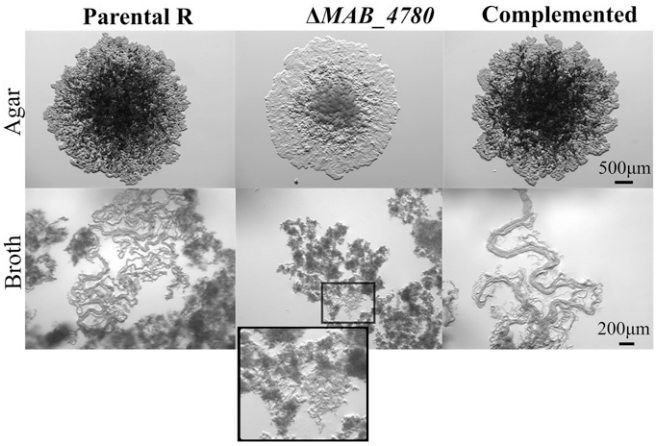

Fig. 3. Disruption of *MAB_4780* correlates with loss of cording in *Mabs* R. Colony morphology of the parental (R strain), Δ*MAB_4780* mutant, and complemented strains grown on LB medium at 37 °C (*Upper*) and cording aspect of all three strains grown in 7H9 broth at 32 °C and observed under the microscope (*Lower*). All images were taken at the same magnification, and an enlarged view of the boxed inset is shown for the mutant.

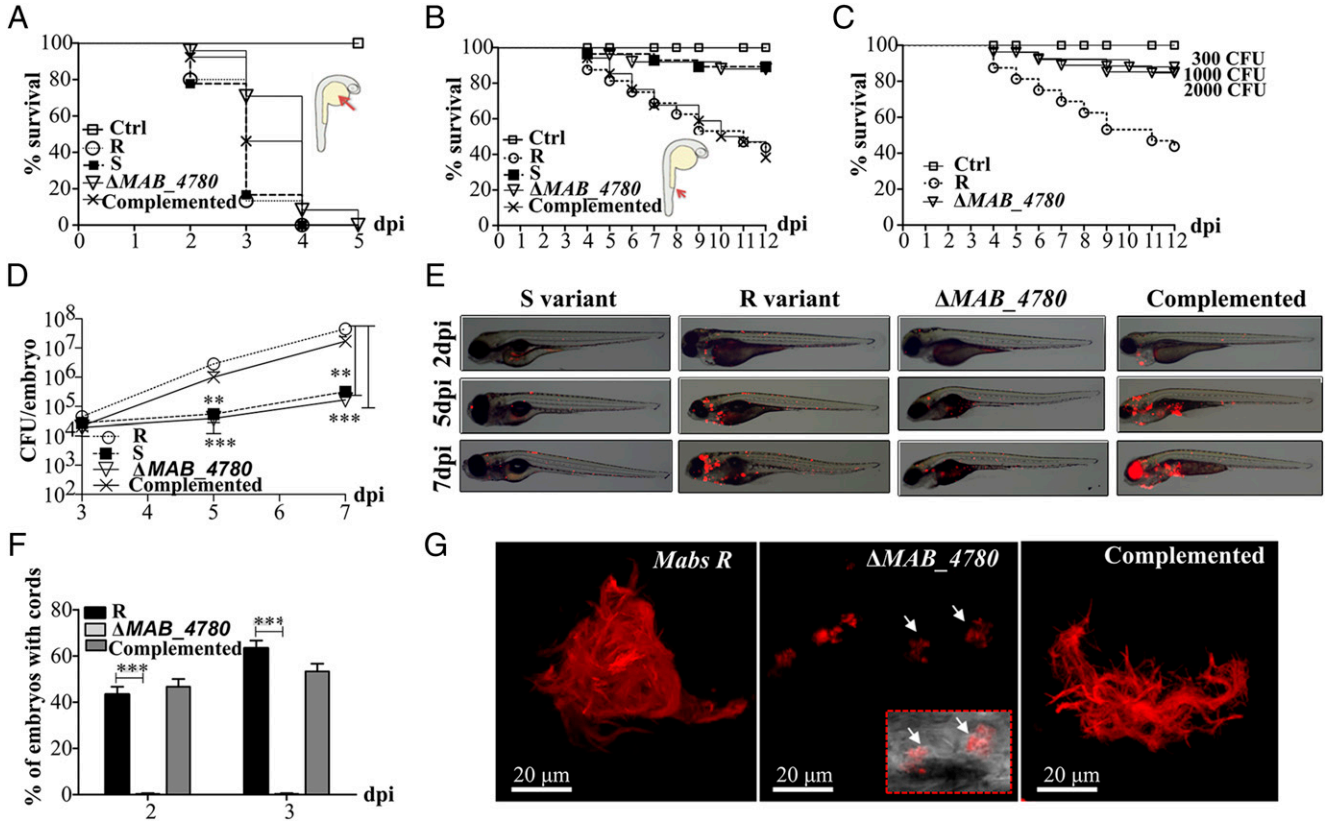

Fig. 4. The Δ*MAB_4780* mutant is extremely attenuated in infected zebrafish embryos. (*A*) Survival curves of embryos injected in the yolk sac (~100–200 cfu) of tdTomato-expressing *Mabs* S, *Mabs* R, Δ*MAB_4780* mutant, or the complemented strain ($n = 20$). There are no significant differences between the different infected strains. Data are representative of three independent experiments. The *Inset* represents an embryo at 30 hpf, and the arrow indicates the injection site in the yolk. Ctrl, noninfected control embryos. (*B*) Survival curve for zebrafish embryos ($n = 20$) injected i.v. at 30 hpf with 100–200 cfu of the different *Mabs* strains compared with control embryos. Larvae infected with the Δ*MAB_4780* mutant showed a significant increase in survival compared with larvae infected with the parental strain ($P = 0.0008$, log-rank test), whereas the complemented strain behaved like the wild-type R variant and restored virulence (no statistically significant differences were seen in the survival of embryos infected with the R or complemented strains; log-rank test). Shown are representative data of three independent experiments. The *Inset* represents an embryo at 30 hpf, and the arrow indicates the caudal vein injection site. (*C*) Survival curve of embryos infected with increasing doses of the Δ*MAB_4780* mutant. Embryos injected with the Δ*MAB_4780* mutant showed no statistically significant difference with the control group in terms of survival, regardless of the dose. Data shown are representative of two independent experiments ($n = 20$). (*D*) In vivo growth of the Δ*MAB_4780* mutant. Enumeration was performed by plating homogenates of whole individual larvae at different time points on selective agar plates and subsequent counting of bacterial colonies. A significant reduction in bacterial burden was observed with the Δ*MAB_4780* mutant (Kruskal–Wallis with Dunn's multiple test; $^{**}P < 0.01$; $^{***}P < 0.001$). Data are representative of three independent experiments. (*E*) Bright field/fluorescence overlay images of tdTomato-labeled *Mabs* (~150 cfu). Each larva was followed and imaged at 2, 5, and 7 dpi. (*F*) Cords were recorded in i.v.-infected embryos with either tdTomato-expressing *Mabs* R, Δ*MAB_4780* mutant, or complemented strains at 2 and 3 dpi. Cords were never observed in Δ*MAB_4780*-infected embryos. Histograms represent means calculated from three independent experiments ($n = 10$ per experiment), and the statistical test used was Fisher's exact test; $^{***}P < 0.001$. Error bars represent the SEM. (*G*) Maximum intensity projection of confocal images showing representative pathological events in 3 dpi embryos i.v.-infected with *Mabs* R, Δ*MAB_4780*, or complemented strains expressing tdTomato (100–200 cfu). Arrows indicate infected cells containing the tdTomato-labeled Δ*MAB_4780* mutant. Only *Mabs* R and complemented strains formed cords.

of larval death at 6 dpi compared with the uninfected embryos (Fig. 6*C*). The cfu plating indicated although the R bacterial counts increased drastically in the *pu.1* morphants, the Δ*MAB_4780* loads increased much slower with a 2 Log reduction in the cfu compared with *Mabs* R (Fig. 6*D*), consistent with whole embryo imaging (Fig. 6*E*). This suggests that the lack of macrophages could not rescue growth and virulence of Δ*MAB_4780*. Importantly, these in vivo conditions stimulating hypercording of the R strain and resulting in acute and lethal infection were not sufficient to promote cording of the mutant, further substantiating a direct correlation between cording and acute infection of *Mabs* R.

Δ*MAB_4780* Infection Is Controlled in Partially Depleted Neutrophil Embryos. That Δ*MAB_4780* remained attenuated even in the absence of macrophages may be explained by the possible role of neutrophils in restricting growth of the mutant. Macrophage-depleted *Tg(mpx:egpf)* embryos, harboring green fluorescent neutrophils, were therefore infected with the tdTomato-expressing bacteria and analyzed by confocal microscopy. Both *Mabs* R and the complemented strain produced cords that were much larger in size than neutrophils and never found to be contained within these cells (Fig. 7*A*). In contrast, Δ*MAB_4780* was mostly present as individual bacilli and essentially contained within neutrophils (Fig. 7*A*), suggesting that, in the absence of macrophages, neutrophils may contribute to the clearance of Δ*MAB_4780*. Consistent with a previous report (37), *csf3r* knockdown clearly reduced the neutrophil population (Fig. 7*B* and Fig. S8*C*) but not the population of macrophages (Fig. S8*D*). Indeed, at 2 dpf and 3 dpf, the *csf3r* morphants displayed a significant reduction of *mpx*-positive neutrophils (about 5 times less in the *csf3r* morphants compared with the wild-type embryos in the trunk and tail) (Fig. 7*B*). *Csf3r* morphants were highly susceptible to *Mabs* R infection with a rapid larval killing (Fig. 7*C*) and exhibited important pathological signs such as abscesses in the central nervous system (Fig. 7*D*), further emphasizing the key role of neutrophils in the control of *Mabs* infection. However, as for the *pu.1* morphants, depletion of the vast majority of neutrophils in the

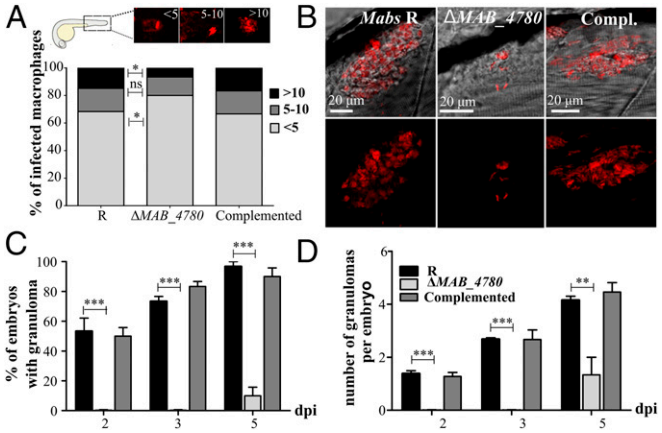

Fig. 5. The intracellular growth defect of Δ*MAB_4780* is associated with impaired granuloma formation in zebrafish. (*A*) Average proportion of infected macrophages classified as mildly, moderately, or highly infected (containing <5, 5–10, and >10 bacteria, respectively) at 24 hpi. Significance was assessed by a Kruskal–Wallis test with Dunn's multiple posttest (*$P < 0.05$). *Top* enclosed panel shows representative infected macrophage of each class. (*B*) Maximum intensity projection of confocal images showing representative granuloma-like structures in 3 dpi larvae i.v.-infected with *Mabs* R, Δ*MAB_4780*, or the complemented strain expressing tdTomato. (*C*) Kinetics of granuloma formation in intravenously-infected embryos (~150 cfu; $n = 30$). Histograms represent means calculated from three independent experiments. Overall, Δ*MAB_4780* mutant-infected embryos developed significantly less granuloma compared with the R and complemented strains. ($n = 30$; Fisher's exact test; ***$P < 0.001$). Error bars represent the SEM. (*D*) Number of granulomas per embryo harboring granuloma. A significant reduction in the number of granulomas per embryo is found in embryos infected with Δ*MAB_4780* compared with R-infected embryos. The statistical test used was the Kruskal–Wallis test with Dunn's multiple posttest ($n = 30$); **$P < 0.01$; ***$P < 0.001$. Error bars represent the SEM.

csf3r morphants failed to rescue virulence of Δ*MAB_4780* (Fig. 7 *C* and *D*), presumably because in the absence of these cells, the sole macrophage population remained efficient in controlling infection of the mutant. Overall, these results indicate that Δ*MAB_4780* is highly attenuated, even in immunocompromized embryos.

Discussion

Analysis of the pathogenicity of *Mabs* has long been hampered by the lack of genetic tools and the restricted panel of cellular/animal models. Making targeted genetic deletions are particularly challenging in the R variant due to its extremely high aggregative properties. Herein, we combined the larval zebrafish as a tractable host to study the innate immune response to *Mabs* (16, 17) and the successful achievement of the first deletion mutant in the R background. We demonstrate that the recombineering method (31) can be successfully applied to inactivate *MAB_4780* in the R variant, leading to multiple and remarkable in vitro and in vivo phenotypes.

Just like in *M. smegmatis*, inactivation of *MAB_4780* led to a higher susceptibility of *Mabs* to TAC. Genetic complementation with either *MAB_4780* or *MSMEG_6754* restored resistance, suggesting a functional redundancy between the two proteins. TAC affects mycolic acid biosynthesis (19–21, 38, 39), suggesting that MAB_4780 may participate in mycolic acid metabolism, despite the fact that all enzymatic steps required for the mycolic acid elongation machinery had been previously identified (40, 41). Compelling evidence indicates that MAB_4780 is a mycolic acid-associated dehydratase: (*i*) Its specific activity is similar to that reported previously for *M. tuberculosis* HadBC dehydratase when using *trans*-2-enoyl-CoA substrates (25); (*ii*) the crystal structure of MAB_4780 is highly similar to the HadAB dehydratases from *M. smegmatis* (28) and *M. tuberculosis* (29); and (*iii*) inactivation of *MAB_4780* correlates with a reduction of the pool of long-chain α-mycolic acids. Our structural mycolic acid analysis indicates that in *Mabs* α-mycolic acids contain mainly 79 carbon atoms, whereas α′-mycolic acids contain 64 carbon atoms. Although α′-mycolic acids can be considered as precursors of the α-mycolic acids, it is not known why these precursors accumulate in some mycobacterial species. A possible explanation could be that HadBC activity may be deficient in these species due to a defect in gene expression or regulation. A mutation or deletion of *hadC* affects the biosynthesis of oxygenated mycolic acids in *M. tuberculosis*, substantially reducing their production and demonstrating the involvement of HadBC in the late elongation steps (22). Combined with our findings that, like HadBC, MAB_4780 exhibits a substrate preference for long fatty acyl chains (C_{12} but not C_4) and that a change in the α/α′-mycolic acid ratio occurs in Δ*MAB_4780*, it can be inferred that MAB_4780 participates also in the last elongation steps of meromycolic acid biosynthesis. However, the presence of these two redundant dehydratases (MAB_4780 and HadBC) in *Mabs* remains puzzling. Perhaps MAB_4780 participates in the elongation step under conditions where HadBC is expressed in limiting concentrations.

Subtle changes in the composition and/or fine structure of the mycolic acids, such as those affecting either the chain length or nature of the chemical functions, can condition their biological activities (42). This may have important consequences like (*i*) the molecular arrangement and fluidity of the mycomembrane and (*ii*) the biological activities of numerous mycolylated cell wall components, usually considered as pathogenic determinants. Among them, trehalose-dimycolate (TDM; also known as cord factor) is implicated in various biological functions, such as pathogenesis, immunomodulation, inflammation, granuloma formation, or cording (43, 44). Strikingly, the cord-deficient phenotype of Δ*MAB_4780* that may directly result from the changes in the mycolic acid pattern provides an ideal tool to unravel the role of cording in pathogenesis of *Mabs* R. Indeed, disruption of *MAB_4780* abrogated all pathophysiological traits of the R strain—virulence, neurotropism, intramacrophage survival, granuloma formation, and cording—emphasizing the critical role of MAB_4780 in pathogenicity of *Mabs* R. It is worth mentioning that mutation/deletion of *hadC* also impacts cording and virulence of *M. tuberculosis* in mice (22), further underlining the redundant functions between MAB_4780 and HadBC. Interestingly, whereas MAB_4780 is needed for cording in *Mabs*, a functional ortholog (MSMEG_6754) is present in the noncording *M. smegmatis* and no orthologs are apparently present in *M. tuberculosis*, a known cording species. This suggests that cording is a complex process that involves a set of genes that are species-specific.

Pathogenic mycobacteria survive within macrophages by residing in phagosomes, which they prevent from maturing and fusing with lysosomes. Mycolic acids are among the bacterial components found to modulate phagosome processing, and recent work has highlighted the importance of PcaA-mediated cyclopropanation of mycolates in prevention of phagosome maturation and intracellular survival of *Mycobacterium bovis* bacillus Calmette–Guérin in human monocyte-derived macrophages (45). Other studies have shown the ability of the surface-exposed TDM to inhibit fusion events between phospholipid vesicles inside host macrophages. Moreover, macrophages incubated with beads coated with a synthetic analog of TDM containing shorter fatty acid chains demonstrated increased colocalization with LysoTracker (46). This implies that the fatty acyl chain length of TDM contributes to the relatively nonfusogenic activity of TDM and may explain the higher proportion of Δ*MAB_4780* that colocalized with acidic vesicles in macrophages. Indeed, the shorter chain length of the Δ*MAB_4780* TDM pool, resulting from the decreased production of long chain α-mycolic acids, may directly affect its capacity to prevent phagolysosomal fusion. This finding, in turn, may explain the poor intramacrophage and intraamoebal survival of the mutant compared with the parental strain, thereby compromising its ability to stimulate early granuloma

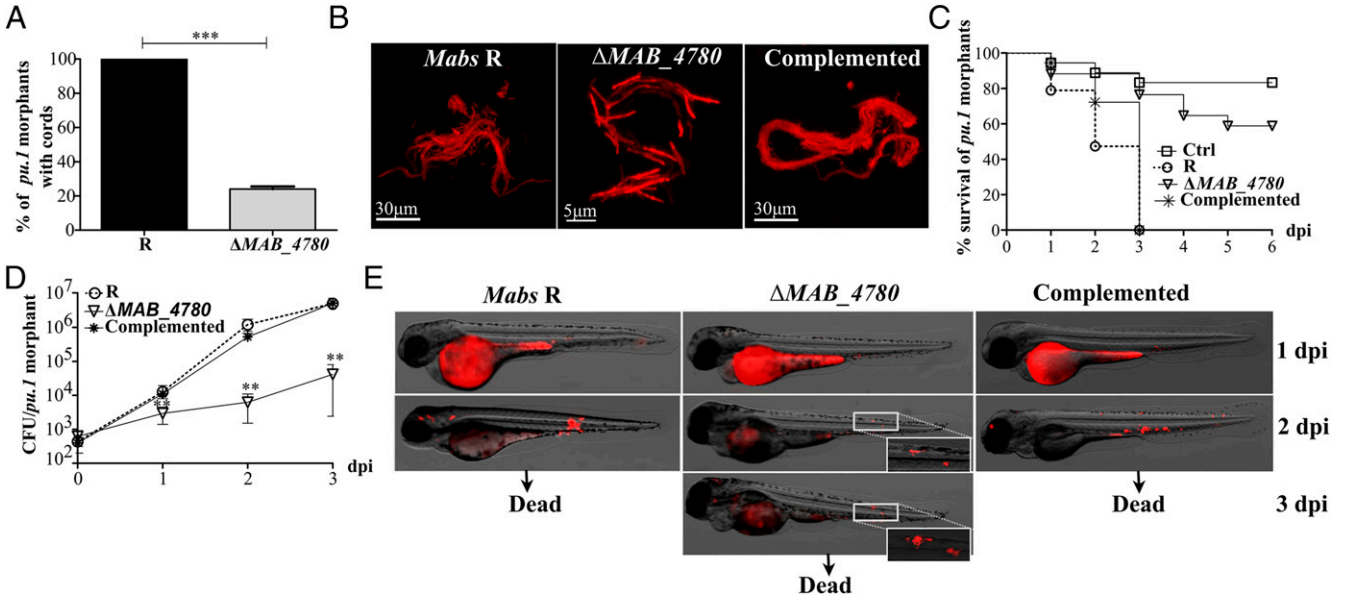

Fig. 6. MABS_4780 is required for acute and lethal zebrafish infection. (*A*) Cords were recorded in *pu.1* embryos infected i.v. with ∼100–200 cfu of either tdTomato-expressing *Mabs* R, Δ*MAB_4780*, or the complemented strain at 2 and 3 dpi ($n = 20$). Percentage of *pu.1* morphants harboring mycobacterial cords after infection with either the R variant or the Δ*MAB_4780* mutant ($n = 20$) at 3 dpi. Data are expressed as means calculated from three independent experiments ($n = 10$ per experiment). The statistical test was Fisher's exact test; $***P < 0.001$. Error bars represent the SEM. (*B*) Maximum intensity projection of confocal images showing representative cords in *pu.1* morphants i.v. infected with the *Mabs* R, Δ*MAB_4780*, and complemented strains expressing tdTomato at 2 dpi (∼150 cfu). Only *Mabs* R and the complemented strain exhibited cords made of structured networks of multiple tight bundles, consisting of end-to-end and side-to-side parallel-aligned bacilli along the long axis of the cord, whereas extracellular growth of Δ*MAB_4780* resulted essentially in size-limited and very thin structures. (*C*) Survival of macrophage-depleted embryos infected with 150 cfu at 30 hpf. Embryos are significantly more susceptible to R infection ($P < 0.0001$, log-rank test) than to Δ*MAB_4780* infection (statistically not different from *pu.1* morphant control). Shown are representative data of three independent experiments. (*D*) Growth kinetic of Δ*MAB_4780* in *pu.1* morphants (∼100–200 cfu). The cfu enumeration showed reduced Δ*MAB_4780* loads compared with R loads ($**P < 0.01$; Mann–Whitney test). Symbols represent means calculated from three independent experiments. Error bars represent the SEM. (*E*) Real-time imaging of *pu.1* morphants infected as in *B*, with special emphasis on cording. Autofluorescence of the yolk is seen at 1 dpi.

formation. Alternatively, because TDM has also been proposed as a potent granulomatogenic component of the cell wall (47), one cannot rule out that the subtle structural modifications affecting TDM in Δ*MAB_4780* may negatively impact granuloma formation.

Another unanticipated finding arising from this work relies on the innate phagocyte populations required to control infection of Δ*MAB_4780*. Depletion of either macrophages or neutrophils rendered host larvae susceptible to invasive disease by the R variant but resulted in an attenuated disease following challenge with the less virulent Δ*MAB_4780* strain. We hypothesize that early interactions between Δ*MAB_4780* and neutrophils in *pu.1* morphants or with macrophages in *csf3r* morphants may contribute to the specific virulence defect for Δ*MAB_4780*, especially considering that this strain has decreased levels of α-mycolic acids, leading to a defect in the shielding hydrophobic cell envelope composition/architecture. However, either macrophages or neutrophils are required to control the infection of Δ*MAB_4780*, as the mutant regains full virulence when injected in the yolk consisting of a single giant cell encapsulated by a plasma membrane and where chemotaxis of phagocytes is impaired. We have previously shown that bacteria released from apoptotic macrophages grow extracellularly and form cords, which subsequently prevent *Mabs* R from being phagocytozed by macrophages and neutrophils (16). The present results suggest that Δ*MAB_4780*, because it is defective in cording, grows as more homogenous nonclustered bacilli, which are rapidly phagocytozed and destroyed by macrophages and neutrophils.

In summary, this study clearly demonstrates that inactivation of the dehydratase MAB_4780 strongly affects *Mabs* R pathogenicity and that attenuation is very likely to result from both cord deficiency and intracellular growth impairment. Because interfering with MAB_4780 results in an extremely attenuated phenotype in multiple cellular and animal hosts, its selective inhibition may represent an original and alternative approach to standard chemotherapy to control invasive and acute *Mabs* infections. Chemical inhibition of MAB_4780 may represent an attractive way to attenuate cording. In this context, the in vitro dehydratase assay combined with our high-resolution crystal structure will be particularly helpful in the process of screening and selecting high-affinity inhibitors. Once obtained, the selected molecules could then be assessed in the *Mabs*/zebrafish system, which has recently been validated as a preclinical animal model to test the in vivo therapeutic efficacy of drugs active against *Mabs* (48, 49). Such advanced strategies are particularly warranted as *Mabs* is refractory to most antibiotics treatments and often associated with high therapeutic failure.

Methods

Bacterial Strains and Growth Conditions. All bacterial strains used in this study are listed in Table S2. For cloning, *Escherichia coli* strains were grown at 37 °C in LB medium with kanamycin (25 μg/mL), hygromycin (25 μg/mL), or ampicillin (200 μg/mL) when required. Mycobacteria were routinely maintained at 32 °C in Middlebrook 7H9 broth supplemented with 10% (vol/vol) oleic acid–albumin–dextrose–catalase (OADC) enrichment and 0.05% Tween 80 or grown on Middlebrook 7H10 agar supplemented with 10% (vol/vol) OADC and appropriate antibiotics. In vitro growth was examined by inoculating the midlog phase culture into fresh 7H9 at an OD_{600} of ∼0.01, followed by regular measurements at different time points, along with enumeration of the cfu on plates. Due to the tendency of *Mabs* to clump, resulting in heterogenous suspensions that may prevent accurate growth determinations, a third method was adopted by monitoring the red fluorescence emitted by the strains carrying pTEC27 (expressing tdTomato).

Plasmids and DNA Manipulation. All plasmids used in this study are listed in Table S2. The pMV306_*4780* construct was made by amplifying *MAB_4780*

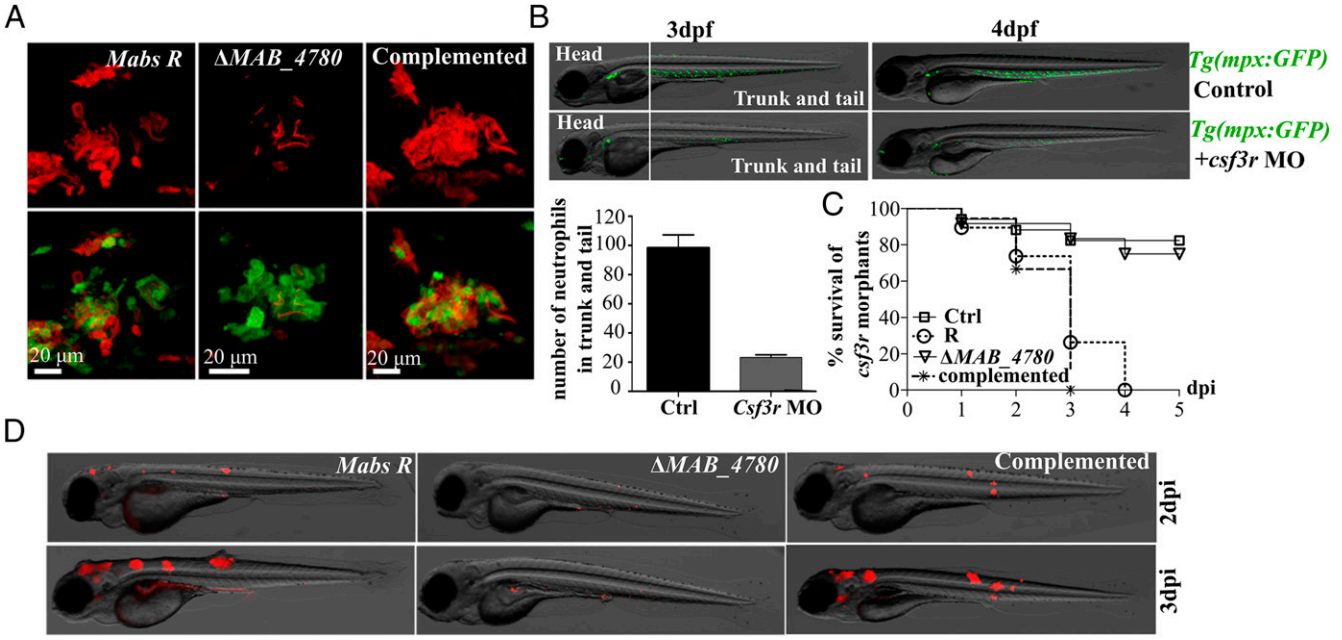

Fig. 7. Virulence of Δ*MAB_4780* is attenuated in a neutrophil-depleted host. (*A*) Maximum intensity projection of confocal images showing representative neutrophil activity (at 2 dpi) in *pu.1 Tg(mpx:egpf)* morphants i.v.-infected with *Mabs* R, Δ*MAB_4780*, or complemented strain expressing tdTomato. (*B*) *Csf3r Tg(mpx:egpf)* morphants showed highly reduced neutrophil numbers at 3 and 4 dpf, confirming the proper activity of the morpholino. The numbers of *mpx*-positive neutrophils counted in the trunk and tail at 3 dpf are depicted in the graph. (*C*) Survival curve of neutrophil-depleted larvae i.v.-infected with the *Mabs* R, Δ*MAB_4780*, and complemented strains (~150 cfu, $n = 20$ per group). These larvae were hypersusceptible to *Mabs* R and to the complemented strain ($P < 0.001$, log-rank test) but not to Δ*MAB_4780* (statistically not different from PBS-injected controls). Shown are representative data from two independent experiments. (*D*) Representative fluorescence and DIC overlays of infected *csf3r* morphants at 2 and 3 dpi.

from *Mabs* R genomic DNA using forward primer (5′-CCCTGGCCATGACTG-CACCAGTAGACGGGTCG-3′; MscI) and reverse primer (5′-CGGGATCCTCA-GCTGAAGCGCACGCTCATCG-3′; BamHI). The amplified product was then ligated into the MscI/BamHI-restricted pMV261. The *MAB_4780* gene along with the *hsp60* promoter was then restricted with XbaI and HindIII and subcloned into the XbaI/HindIII-digested pMV306, yielding pMV306_*4780*. To generate pMV206_Apra_*tdTomato*, the *tdTomato* gene was excised from pTEC27 using MfeI/NheI and directly ligated into the MfeI/XbaI-restricted pMV206_Apra. Constructs were verified by DNA sequencing.

Construction of Δ*MAB_4780* Deletion Mutant. All genetic manipulations in *Mabs* R were carried out using the recombineering technique (31). Briefly, an allelic exchange substrate for the *MAB_4780* gene deletion was prepared by amplifying the left and right flanking arms and cloning them on either side of the hygromycin-resistant gene in the shuttle vector pJSC347. The left arm was directly cloned using SpeI and HindIII sites and the right arm using XbaI and KpnI. The allelic exchange substrate was then excised from the vector backbone by digesting with SpeI and AflII and directly electroporated into freshly prepared electrocompetent *Mabs* R cells carrying pJV53-Zeo (31). Plates were incubated at 37 °C for 1 week, and colonies resistant to zeocin and hygromycin were screened by PCR for correct gene replacement. Primers used to amplify the left and right arms are listed in Table S3.

Susceptibility to SDS and TAC. Susceptibility of *Mabs* to SDS or TAC was assessed visually on Middlebrook 7H10/OADC plates containing increasing detergent or drug concentrations, as reported earlier (50). Tenfold serial dilutions of actively growing culture were plated and incubated at 37 °C for 4–5 d. The minimal inhibitory concentration (MIC) was defined as the minimum concentration required to inhibit 99% of the bacterial growth. Drug susceptibility testing was also determined using the microdilution method, in cation-adjusted Mueller–Hinton broth, according to the Clinical and Laboratory Standards Institute guidelines (51).

***Mycobacterium* Preparations for Infection Studies.** Cultures were grown to midlog phase, pelleted, washed twice, and resuspended in PBS supplemented with 0.05% Tween-80 (PBS^T). Bacterial clumps were disrupted by 10 successive passages through a 26-gauge needle and sonicated three times for 10 s each to disperse bacteria. Remaining clumps were allowed to sediment by centrifugation at 150 × *g* for 1 min. The OD was then measured at 600 nm to adjust the final concentration of the bacteria.

Macrophage Infections. Murine J774 macrophages were grown at 37 °C in a 5% CO_2 incubator in DMEM supplemented with 10% (vol/vol) FBS. Cells were seeded 24 h before infection at 1×10^5 cells/mL. Bacteria were added at a multiplicity of infection (MOI) of 1. After 3 h of infection, extracellular mycobacteria were removed by washing before adding fresh medium containing 250 μg/mL of amikacin for 1 h. Fresh medium containing 50 μg/mL of amikacin was then added. For cfu determination, cells were lysed with 1% Triton X-100 in PBS, and bacteria were quantified after plating serial dilutions of lysates on 7H10 plates and incubation at 37 °C.

Zebrafish Manipulation and Infection Studies. All zebrafish experiments were approved by the Direction Sanitaire et Vétérinaire de l'Hérault and Comité d'Ethique pour l'Expérimentation Animale de la région Languedoc Roussillon under the reference CEEA-LR- CEEALR36-1145. Experiments were done using the golden zebrafish mutant (52), the Tg(*mpeg1:mCherryF*) to visualize macrophages (16), or the Tg (*mpx:egfp*) to visualize neutrophils (53). Bacteria were adjusted to an OD_{600} of 1 in PBS^T and mixed with phenol red. Microinjections of ~2–3 nL of bacterial suspensions, containing around 150 bacteria, were done directly into the bloodstream or into the yolk sac of 30 hpf dechorionated and anesthetized embryos. To determine the survival curves, infected larvae were transferred into individual wells and incubated at 32 °C. Mortality was determined by recording the number of dead embryos daily. To monitor the bacterial loads, groups of three infected embryos were collected at different time points, lysed individually in 2% (vol/vol) Triton X-100, and homogenized though a 26-gauge needle and the homogenates were serially diluted and plated on Middlebrook 7H10/OADC supplemented with BBL MGIT PANTA (BD) (16).

Microinjection of Antisense Morpholinos. Oligonucleotide morpholinos consisting of splice-blocking 5′-GGTCTTTCTCCTTACCATGCTCTCC-3′ and ATG 5′-CCTCCATTCTGTACGGATGCAGCAT-3′ morpholinos against *pu.1* (Gene Tools) were combined to final concentrations of 0.025 mM and 0.375 mM, respectively (36). Transient depletion of the neutrophils was performed in the transgenic Tg(*mpeg:mcherry*) zebrafish line using the *csf3r* morpholino

5′-TTTGTCTTTACAGATCCGCCAGTTC-3′ (Gene Tools) at 0.7 mM. Morpholino solutions were injected (2–3 nL) into one-cell stage embryos (37).

Live Imaging and Confocal Microscopy. For live imaging, tricaine-anesthetized infected embryos were mounted in 1% low-melting point agarose in a 35-mm Petri dish. Direct observations were performed using a Zeiss microscope with a Zeiss Plan Neo Fluor Z 1×/0.25 objective and equipped with an AxioCam 503 monochrom camera (Zeiss) and acquired and processed with ZEN 2 software (blue edition). For confocal microscopy, anesthetized embryos were fixed overnight at 4 °C with 4% (vol/vol) paraformaldehyde (PAF) in PBS^T, washed twice in PBS^T, and incubated successively in increasing glycerol concentration up to 50% to preserve the integrity of the tissues. Fixed embryos were then moved onto depressed transparent slides, covered with a coverslip for observation with a 40× Leica Apo oil 1.15 NA objective, and visualized using a Leica DM2500CSQ upright microscope equipped with a Leica TCS SPE confocal scan head as well as fluorescence and differential interference contrast (DIC) optics. Fluorescence and DIC images were acquired and assembled.

Lysotracker Red. LysoTracker Red DND-99 is an acidotropic fluorescent probe that was used as a marker of phagosomal acidification and maturation (54). J774A cells were seeded onto glass coverslips and infected with Fluorescein isothiocyanate, FITC-labeled *Mabs* R, Δ*MAB_4780*, and complemented strains (55). In brief, bacterial cultures were suspended in 7H9 broth and labeled with 100 μg/mL of FITC for 2 h at room temperature (RT) with gentle agitation in the darkness. FITC-labeled bacteria were washed once with 7H9 broth supplemented with 4% (wt/vol) BSA and then twice with 7H9 broth without BSA. The final concentration of the bacteria was assessed by measuring OD_{600}, and infection was done at an MOI of 1:1. After 3 h of infection, cells were washed twice with DMEM to remove extracellular bacteria and incubated with DMEM containing 1 μM LysoTracker Red DND-99 (Molecular Probes) for 30 min at 37 °C. Subsequently, cells were washed three times with PBS and fixed with 4% (vol/vol) PAF for microscopy. The *z* stacks were acquired using a Zeiss Axio Imager Z2 equipped with an Orca flash 4.0 sCMOS camera (Hamamatsu) and with an Apotome (Zeiss) for optical slicing, using a 100× NA 1.4 Apochromat objective. Images were processed for luminosity–contrast adjustment with Zen Software (Zeiss). Colocalization was counted via Fiji. At least 100 phagosomes were counted for each strain performed in two independent experiments.

Expression and Purification of MAB_4780. *MAB_4780* was cloned into the BamHI/XhoI-restricted pET32a(+) (Novagen) allowing the gene to be in frame with the S-, hexa-histidine, and thioredoxin tags. A Tobacco Etch Virus (TEV) protease cleavage site was added between the tags for subsequent removal of the tags during the purification process. MAB_4780 was expressed in *E. coli* BL21 Rosetta 2 as follows. An overnight preculture grown in LB supplemented with ampicillin and chloramphenicol was used to inoculate 4 L of LB supplemented with both antibiotics. Cultures were grown at 37 °C to 0.8 OD_{600}, and protein expression was induced with 1 mM IPTG, overnight (ON) at 16 °C. Bacteria were harvested; resuspended in lysis buffer containing 50 mM Tris·HCl, pH 8, 0.4 M NaCl, 5 mM β-mercaptoethanol, 20 mM imidazole, and 1 mM benzamidine; and disrupted by four cycles of 2 min sonication before centrifugation for 35 min at 30,000 × *g*. The resulting supernatant was loaded onto a 3 mL Sepharose nickel affinity column using gravity. Beads were washed with five volumes of lysis buffer and then with five volumes of 50 mM Tris·HCl, pH 8, and 1 M NaCl. Protein elution was done with three volumes of 50 mM Tris·HCl, pH 8, 0.2 M NaCl, 5 mM β-mercaptoethanol, 400 mM imidazole, and 1 mM benzamidine. The eluted protein was then mixed with TEV in a 1:50 (wt/wt) ratio; dialyzed ON at 4 °C against 50 mM Tris·HCl, pH 8, 0.2 M NaCl, and 5 mM β-mercaptoethanol; and subjected to a second nickel affinity chromatography column to release the tag-free protein in the flow-through. The protein was concentrated to 5 mg/mL and subjected to a size exclusion chromatography onto an ENrichTM SEC 650 column (Biorad). Purity was estimated around 95% by SDS/PAGE.

Size Exclusion Chromatography. A calibration curve was obtained using the Gel Filtration Markers Kit for Protein Molecular Weights 12,400–200,000 Da (Sigma-Aldrich) by plotting the partition coefficient K_{av} against the logarithms of the molecular weight of standard proteins. The void volume was determined with blue dextran. Proteins were loaded onto an ENrichTM SEC 650 column (Biorad) and eluted with buffer containing 50 mM Tris·HCl, pH 8, 200 mM NaCl, and 5 mM β-mercaptoethanol at a flow rate of 0.5 mL/min at RT.

Synthesis of 2-*Trans*-Enoyl-CoA Substrates. To a solution of 2-*trans*-octenoic acid or 2-*trans*-dodecenoic acid (0.55 mmol) in *t* butyl methyl ether (14 mL) we added diisopropylethylamine (0.1 mL, 0.57 mmol) and ethyl chloroformate (0.1 mL, 0.52 mmol). The suspension was stirred at RT overnight under nitrogen, filtered, and evaporated to dryness. A solution of CoA sodium salt (50 mg, 0.06 mmol) in 0.3 M aqueous sodium bicarbonate solution/95% (vol/vol) EtOH/ethyl acetate (1/1/1; vol/vol/vol; 6 mL) was added dropwise to the residue. The reaction mixture was stirred for 1 h at RT and quenched with acetic acid (0.1 mL). After three extractions with ethyl acetate, the aqueous phase was lyophilized, and the 2-*trans*-enoyl-CoAs were purified by HPLC on a C18 reverse phase column. The column was pre-equilibrated before the injection for 10 min with H_2O/CH_3OH/10% (vol/vol) CH_3OH in 0.1 M NaH_2PO_4 (72/8/20, vol/vol/vol) at a flow rate of 3 mL/min. For purification of the enoyl-CoAs, the flow rate was set at 1 mL/min and the wavelength at 260 nm. The mobile phase was H_2O/CH_3OH 90/10 (vol/vol) with a linear increase to 30% (vol/vol) CH_3OH in 30 min. Crotonoyl-CoA was purchased from Sigma-Aldrich.

Dehydratase Assay. The dehydratase activity was assayed as the decrease of the OD_{263} nm corresponding to the disappearance of the double bond, where a loss of 0.67 OD corresponds to a product concentration of 100 μM. The reaction mixture contained 20 mM potassium phosphate buffer at pH 7, 100 μM of enoyl-CoA, and 430 nM of enzyme. The reaction was assayed in a 1 mL quartz cuvette at 25 °C in a NanoDrop 2000c spectrophotometer (Thermo Scientific).

Crystallization, Data Collection, and Structure Refinement. The protein concentrated to 5 mg/mL and in the presence of 2 mM *trans*-2-dodecanoyl-CoA was crystallized in 0.1 M Tris·HCl, pH 8.5 ,and 2.8 M AmSO4 in sitting drops at 18 °C. Crystals were cryocooled in liquid nitrogen without any cryoprotecting solution before data collection. A full dataset was collected at the BM30 beamline [European Synchrotron Radiation Facility (ESRF)]. The data collection statistics are reported in Table S1. The structure was solved by molecular replacement using Phaser from the Phenix package (56) and using as search model for the structure of the *M. smegmatis* MSMEG_6754 protein [Protein Data Bank (PDB) ID code 4v12] (23). Refinement and model quality were done using the Phenix package (56), and the model building was performed with COOT (57). Figures were made using Pymol.

Production of Polyclonal Anti-MAB_4780 Antibodies and Western Blotting. Polyclonal antibodies against recombinant MAB_4780 were generated in BALB/c mice (Janvier) according to standards protocols. Antigen (20 μg per mice) diluted in PBS was emulsified at a 1/1 proportion in incomplete Freund's adjuvant. Mice were s.c. immunized (final volume of 200 μL) at multiple sites, at days 1, 28, and 57. Blood samples were collected 1 wk after the last immunization from the retro-orbital plexus, and sera were stored at −20 °C until use. Animal experiments were performed according to institutional and national ethical guidelines (Agreement no. 92-033-01, Préfecture des Hauts de Seine, Boulogne, France). For Western blotting, bacteria were harvested, resuspended in PBS, and disrupted by bead beating with 1-mm diameter glass beads. Protein concentration for the resulting lysates was determined using the BCA Protein Assay Reagent kit (Pierce), according to the manufacturer's instructions. Equal amounts of proteins (35 μg) were subjected to SDS/PAGE separation and then transferred to a nitrocellulose membrane. For detection of MAB_4780, the membrane was incubated overnight with the mouse anti-MAB_4780 antibody (dilution 1:1,000), washed, and subsequently incubated with goat anti-mouse antibody conjugated to peroxidase (Jackson ImmunoResearch Laboratories). The signal was revealed using the Luminata Forte Western HRP substrate (Millipore).

Statistical Analysis. All statistical analyses were performed using GraphPad Prism 5 (Graphpad Software). Comparison between survival curves was performed using the log rank test. The cfu counts were analyzed using the Mann–Whitney *t* test when comparing two groups or one-way ANOVA (Kruskal–Wallis with Dunn's multiple test) when comparing more than two groups. For the quantification experiments, Fisher's exact test was used. Only P values < 0.05 were considered as statistically significant.

ACKNOWLEDGMENTS. The authors thank J. P. Levraud for the generous gift of *csf3r* morpholinos. We also thank the staff at ESRF for their help during X-ray data collection. This study was supported by the French National Research Agency (DIMYVIR ANR-13-BSV3-0007-01), the Labex EpiGenMed (I.H.), the Fondation de France (S.C.-K.), and the InfectioPôle Sud (A.V.). L.K. acknowledges the support of Fondation pour la Recherche Médicale (FRM) Grant DEQ20150331719.

1. Middlebrook G, Dubos RJ, Pierce C (1947) Virulence and morphological characteristics of mammalian tubercle bacilli. *J Exp Med* 86(2):175–184.
2. Kaminski DA, Hardy DJ (1995) Selective utilization of DNA probes for identification of Mycobacterium species on the basis of cord formation in primary BACTEC 12B cultures. *J Clin Microbiol* 33(6):1548–1550.
3. McCarter YS, Ratkiewicz IN, Robinson A (1998) Cord formation in BACTEC medium is a reliable, rapid method for presumptive identification of Mycobacterium tuberculosis complex. *J Clin Microbiol* 36(9):2769–2771.
4. Grosset J (2003) Mycobacterium tuberculosis in the extracellular compartment: An underestimated adversary. *Antimicrob Agents Chemother* 47(3):833–836.
5. Staropoli JF, Branda JA (2008) Cord formation in a clinical isolate of Mycobacterium marinum. *J Clin Microbiol* 46(8):2814–2816.
6. Julián E, et al. (2010) Microscopic cords, a virulence-related characteristic of Mycobacterium tuberculosis, are also present in nonpathogenic mycobacteria. *J Bacteriol* 192(7):1751–1760.
7. Medjahed H, Gaillard J-L, Reyrat J-M (2010) Mycobacterium abscessus: A new player in the mycobacterial field. *Trends Microbiol* 18(3):117–123.
8. Nessar R, Cambau E, Reyrat JM, Murray A, Gicquel B (2012) Mycobacterium abscessus: A new antibiotic nightmare. *J Antimicrob Chemother* 67(4):810–818.
9. Koh W-J, et al. (2006) Clinical significance of nontuberculous mycobacteria isolated from respiratory specimens in Korea. *Chest* 129(2):341–348.
10. Parkins MD, Floto RA (2015) Emerging bacterial pathogens and changing concepts of bacterial pathogenesis in cystic fibrosis. *J Cyst Fibros* 14(3):293–304.
11. Torres-Coy JA, Rodríguez-Castillo BA, Pérez-Alfonzo R, DE Waard JH (2016) Source investigation of two outbreaks of skin and soft tissue infection by Mycobacterium abscessus subsp. abscessus in Venezuela. *Epidemiol Infect* 144(5):1117–1120.
12. Howard ST, et al. (2006) Spontaneous reversion of Mycobacterium abscessus from a smooth to a rough morphotype is associated with reduced expression of glycopeptidolipid and reacquisition of an invasive phenotype. *Microbiology* 152(Pt 6): 1581–1590.
13. Medjahed H, Reyrat J-M (2009) Construction of Mycobacterium abscessus defined glycopeptidolipid mutants: comparison of genetic tools. *Appl Environ Microbiol* 75(5): 1331–1338.
14. Pawlik A, et al. (2013) Identification and characterization of the genetic changes responsible for the characteristic smooth-to-rough morphotype alterations of clinically persistent Mycobacterium abscessus. *Mol Microbiol* 90(3):612–629.
15. Bernut A, et al. (2016) Insights into the smooth-to-rough transitioning in Mycobacterium bolletii unravels a functional Tyr residue conserved in all mycobacterial MmpL family members. *Mol Microbiol* 99(5):866–883.
16. Bernut A, et al. (2014) Mycobacterium abscessus cording prevents phagocytosis and promotes abscess formation. *Proc Natl Acad Sci USA* 111(10):E943–E952.
17. Bernut A, et al. (2015) Deciphering and imaging pathogenesis and cording of Mycobacterium abscessus in zebrafish embryos. *J Vis Exp* 103(103):e53130.
18. Glickman MS, Cox JS, Jacobs WR, Jr (2000) A novel mycolic acid cyclopropane synthetase is required for cording, persistence, and virulence of Mycobacterium tuberculosis. *Mol Cell* 5(4):717–727.
19. Belardinelli JM, Morbidoni HR (2012) Mutations in the essential FAS II β-hydroxyacyl ACP dehydratase complex confer resistance to thiacetazone in Mycobacterium tuberculosis and Mycobacterium kansasii. *Mol Microbiol* 86(3):568–579.
20. Grzegorzewicz AE, et al. (2012) A common mechanism of inhibition of the Mycobacterium tuberculosis mycolic acid biosynthetic pathway by isoxyl and thiacetazone. *J Biol Chem* 287(46):38434–38441.
21. Coxon GD, et al. (2013) Synthesis, antitubercular activity and mechanism of resistance of highly effective thiacetazone analogues. *PLoS One* 8(1):e53162.
22. Slama N, et al. (2016) The changes in mycolic acid structures caused by *hadC* mutation have a dramatic effect on the virulence of Mycobacterium tuberculosis. *Mol Microbiol* 99(4):794–807.
23. Carrère-Kremer S, et al. (2015) A new dehydratase conferring innate resistance to thiacetazone and intra-amoebal survival of Mycobacterium smegmatis. *Mol Microbiol* 96(5):1085–1102.
24. Rock CO, Cronan JE (1996) Escherichia coli as a model for the regulation of dissociable (type II) fatty acid biosynthesis. *Biochim Biophys Acta* 1302(1):1–16.
25. Sacco E, et al. (2007) The missing piece of the type II fatty acid synthase system from Mycobacterium tuberculosis. *Proc Natl Acad Sci USA* 104(37):14628–14633.
26. Yang M, Guja KE, Thomas ST, Garcia-Diaz M, Sampson NS (2014) A distinct MaoC-like enoyl-CoA hydratase architecture mediates cholesterol catabolism in Mycobacterium tuberculosis. *ACS Chem Biol* 9(11):2632–2645.
27. Koski KM, Haapalainen AM, Hiltunen JK, Glumoff T (2005) Crystal structure of 2-enoyl-CoA hydratase 2 from human peroxisomal multifunctional enzyme type 2. *J Mol Biol* 345(5): 1157–1169.
28. Biswas R, et al. (2015) Crystal structure of dehydratase component HadAB complex of mycobacterial FAS-II pathway. *Biochem Biophys Res Commun* 458(2):369–374.
29. Dong Y, et al. (2015) Molecular basis for the inhibition of β-hydroxyacyl-ACP dehydratase HadAB complex from Mycobacterium tuberculosis by flavonoid inhibitors. *Protein Cell* 6(7):504–517.
30. Krissinel E (2015) Stock-based detection of protein oligomeric states in jsPISA. *Nucleic Acids Res* 43(W1):W314–W319.
31. van Kessel JC, Hatfull GF (2007) Recombineering in Mycobacterium tuberculosis. *Nat Methods* 4(2):147–152.
32. Prajsnar TK, Cunliffe VT, Foster SJ, Renshaw SA (2008) A novel vertebrate model of Staphylococcus aureus infection reveals phagocyte-dependent resistance of zebrafish to non-host specialized pathogens. *Cell Microbiol* 10(11):2312–2325.
33. van der Sar AM, et al. (2003) Zebrafish embryos as a model host for the real time analysis of Salmonella typhimurium infections. *Cell Microbiol* 5(9):601–611.
34. Drancourt M (2014) Looking in amoebae as a source of mycobacteria. *Microb Pathog* 77:119–124.
35. Deretic V, Fratti RA (1999) Mycobacterium tuberculosis phagosome. *Mol Microbiol* 31(6):1603–1609.
36. Clay H, et al. (2007) Dichotomous role of the macrophage in early Mycobacterium marinum infection of the zebrafish. *Cell Host Microbe* 2(1):29–39.
37. Palha N, et al. (2013) Real-time whole-body visualization of Chikungunya Virus infection and host interferon response in zebrafish. *PLoS Pathog* 9(9):e1003619.
38. Alahari A, et al. (2007) Thiacetazone, an antitubercular drug that inhibits cyclopropanation of cell wall mycolic acids in mycobacteria. *PLoS One* 2(12):e1343.
39. Alahari A, et al. (2009) Mycolic acid methyltransferase, MmaA4, is necessary for thiacetazone susceptibility in Mycobacterium tuberculosis. *Mol Microbiol* 71(5): 1263–1277.
40. Marrakchi H, Lanéelle M-A, Daffé M (2014) Mycolic acids: Structures, biosynthesis, and beyond. *Chem Biol* 21(1):67–85.
41. Pawełczyk J, Kremer L (2014) The molecular genetics of mycolic acid biosynthesis. *Microbiol Spectr* 2(4):MGM2-0003-2013.
42. Verschoor JA, Baird MS, Grooten J (2012) Towards understanding the functional diversity of cell wall mycolic acids of Mycobacterium tuberculosis. *Prog Lipid Res* 51(4): 325–339.
43. Hunter RL, Olsen MR, Jagannath C, Actor JK (2006) Multiple roles of cord factor in the pathogenesis of primary, secondary, and cavitary tuberculosis, including a revised description of the pathology of secondary disease. *Ann Clin Lab Sci* 36(4):371–386.
44. Rao V, Fujiwara N, Porcelli SA, Glickman MS (2005) Mycobacterium tuberculosis controls host innate immune activation through cyclopropane modification of a glycolipid effector molecule. *J Exp Med* 201(4):535–543.
45. Corrales RM, et al. (2012) Phosphorylation of mycobacterial PcaA inhibits mycolic acid cyclopropanation: consequences for intracellular survival and for phagosome maturation block. *J Biol Chem* 287(31):26187–26199.
46. Indrigo J, Hunter RL, Jr, Actor JK (2003) Cord factor trehalose 6,6′-dimycolate (TDM) mediates trafficking events during mycobacterial infection of murine macrophages. *Microbiology* 149(Pt 8):2049–2059.
47. Geisel RE, Sakamoto K, Russell DG, Rhoades ER (2005) In vivo activity of released cell wall lipids of Mycobacterium bovis bacillus Calmette-Guérin is due principally to trehalose mycolates. *J Immunol* 174(8):5007–5015.
48. Bernut A, et al. (2014) In vivo assessment of drug efficacy against Mycobacterium abscessus using the embryonic zebrafish test system. *Antimicrob Agents Chemother* 58(7):4054–4063.
49. Dubée V, et al. (2015) β-Lactamase inhibition by avibactam in Mycobacterium abscessus. *J Antimicrob Chemother* 70(4):1051–1058.
50. Dover LG, et al. (2007) EthA, a common activator of thiocarbamide-containing drugs acting on different mycobacterial targets. *Antimicrob Agents Chemother* 51(3): 1055–1063.
51. Woods GL, et al. (2011) *Susceptibility Testing of Mycobacteria, Nocardiae and Other Aerobic Actinomycetes: Approved Standard* (Clinical and Laboratory Standards Institute, Wayne, PA), 2nd Ed, pp M24–A2.
52. Lamason RL, et al. (2005) SLC24A5, a putative cation exchanger, affects pigmentation in zebrafish and humans. *Science* 310(5755):1782–1786.
53. Renshaw SA, et al. (2006) A transgenic zebrafish model of neutrophilic inflammation. *Blood* 108(13):3976–3978.
54. Toyooka K, Takai S, Kirikae T (2005) Rhodococcus equi can survive a phagolysosomal environment in macrophages by suppressing acidification of the phagolysosome. *J Med Microbiol* 54(Pt 11):1007–1015.
55. Brzostek A, et al. (2014) Either non-homologous ends joining or homologous recombination is required to repair double-strand breaks in the genome of macrophage-internalized Mycobacterium tuberculosis. *PLoS One* 9(3):e92799.
56. Adams PD, et al. (2010) PHENIX: A comprehensive Python-based system for macromolecular structure solution. *Acta Crystallogr D Biol Crystallogr* 66(Pt 2):213–221.
57. Emsley P, Lohkamp B, Scott WG, Cowtan K (2010) Features and development of Coot. *Acta Crystallogr D Biol Crystallogr* 66(Pt 4):486–501.
58. Snapper SB, Melton RE, Mustafa S, Kieser T, Jacobs WR, Jr (1990) Isolation and characterization of efficient plasmid transformation mutants of Mycobacterium smegmatis. *Mol Microbiol* 4(11):1911–1919.
59. Stoop EJM, et al. (2011) Zebrafish embryo screen for mycobacterial genes involved in the initiation of granuloma formation reveals a newly identified ESX-1 component. *Dis Model Mech* 4(4):526–536.
60. Stover CK, et al. (1991) New use of BCG for recombinant vaccines. *Nature* 351(6326): 456–460.